phys. stat. sol. (b) **233**, No. 1, 49–58 (2002)

Atomistic Simulations with Carbon Nanotubes – Classical, Quantum, and Transport Modeling

A. MAITI[1]) (a), J. ANDZELM (a), A. SVIZHENKO (b), M. P. ANANTRAM (b), and M. IN HET PANHUIS (c)

(a) Accelrys Inc., 9685 Scranton Road, San Diego, CA 92121, USA

(b) NASA Ames Research Center, Mail Stop: T27A-1, Moffett Field, CA 94035-1000, USA

(c) Materials Ireland Polymer Research Center, Department of Physics, Trinity College, Dublin 2, Ireland

(Received March 15, 2002; accepted May 25, 2002)

PACS: 62.25.+g; 71.15. –m; 73.22.–f; 73.63.Fg

Theoretical modeling of carbon nanotubes continues to provide useful insight and guidance to many experimental efforts toward technological applications. Molecular modeling tools have been used to study important structural, electronic, elastic, transport, and growth properties of nanotubes. We report results from three recent simulations: (i) effect of adsorbates on field emission from a nanotube tip; (ii) effect of mechanical deformation and chirality of nanotubes on electronic transport; and (iii) coating and solubilizing nanotubes by a polymer. The reported simulations are based on first principles density functional theory (DFT), classical molecular mechanics, and tight-binding transport based on the Green's function formalism.

1. Introduction

Ever since their discovery in the early 1990s [1, 2], carbon nanotubes have captured the imagination of researchers worldwide. More recent experimental breakthroughs leading to realistic possibilities of near-term commercial applications [3] have thrust nanotubes as a mainstream research topic both in the basic sciences and in the applied disciplines. Some of the more promising application areas include: field emission based flat panel displays [4], novel semiconducting devices in microelectronics [5, 6], hydrogen storage devices [7], structural reinforcement agents [8], chemical sensors [9], and ultra-sensitive electromechanical sensors [9]. The present paper reviews our modeling endeavor in three areas: (i) effect of adsorbed molecules on the field emission from a metallic nanotube tip, (ii) effect of mechanical deformation and chirality on the electrical conductance of nanotubes, and (iii) coating of a nanotube with a polymer film thereby rendering it soluble in toluene.

2. Computational Methodologies

Different problems require different computational and modeling approaches depending upon the model size and the properties of interest. The three applications described below all required their own set of simulation methodologies and parameter settings. For the first application, i.e., adsorption of molecules at nanotube tips, the number of atoms at the tube tip were limited to 60. Besides, this entailed a study of accurate bind-

[1]) Corresponding author; e-mail: amaiti@accelrys.com

© 2002 WILEY-VCH Verlag GmbH & Co. KGaA, Weinheim 0370-1972/02/23309-0049 $ 17.50+.50/0

ing energy and the effect of the adsorbate on the highest occupied molecular orbital (HOMO). This called for an accurate first principles quantum mechanical (QM) method. We used the DFT code DMol^3 [10] distributed by Accelrys Inc. The electronic wave functions were expanded in a double-numeric polarized (DNP) basis set, the best basis set available with the code. To save computational time, the basis functions were truncated beyond a cutoff distance of 4.0 Å. An all-electron calculation was carried out on a "medium" integration grid using a gradient-corrected PBE exchange-correlation functional [11].

The second application investigated the structure of nanotubes under deformation by an AFM tip. Such large deformation has the potential of altering the chemical bonding, especially in the middle part of the tube right on top of the AFM tip. In this application we are dealing with rather long tubes (2400 atoms), which are much too large for a first principles treatment. Besides, the part of the tube away from the AFM tip is under a simple tensile strain, which can be adequately described by classical molecular mechanics (MM) using an interatomic potential. For this application, we used a QM description of the middle part of the tube, and an MM description of the part away from the AFM tip. The QM code used was DMol^3, as in the first application. However, since the QM system was somewhat larger in this case than the first application (the biggest cluster studied was ~160 atoms), we used the Harris functional [12] for the DFT Hamiltonian. The MM engine used was the Open Force Field (OFF) available through Accelrys' Cerius^2 interface [13]. The interatomic C–C potential was described by the Universal Forcefield (UFF) [14], which has previously been used to study the mechanical properties of carbon nanotubes [15].

The second application also required computing the phase-coherent transport through nanotubes of different chiralities under various deformation conditions. The transmission and conductance were computed using the recursive Green's function formalism [16, 17] using a framework of a nearest-neighbor sp^3-tight-binding Hamiltonian in a non-orthogonal basis. Effects of strain on conductance was accounted for by a bond-length-dependence of the Hamiltonian and the overlap matrices H_{ij} and S_{ij}, as in Ref. [18]. First, the retarded Green's function G^R of the whole nanotube was determined by solving the equation

$$(ES_{ij} - H_{ij} - \sum_{L,ij}^{R} - \sum_{R,ij}^{R}) G^{R,jk} = \delta_i^k \,, \tag{1}$$

where $\sum_{L,R}^{R}$ are the retarded self-energies of the left and the right semi-infinite contacts. The transmission at each energy were then found [19, 20] from the equation

$$T(E) = G^{R,ij} \Gamma_{L,jk} G^{A,kl} \Gamma_{R,li} \,, \tag{2}$$

where $\Gamma_{L,R} = \mathrm{i}\,(\sum_{L,R}^{R} - \sum_{L,R}^{A})$ are the couplings to the left and right leads. Finally, the total conductance of the tube was computed using the Landauer–Büttiker formula

$$G = \frac{2e^2}{h} \int_{-\infty}^{\infty} T(E) \left(-\frac{\partial f_0}{\partial E} \right) \mathrm{d}E \,, \tag{3}$$

where $f_0(E)$ is the Fermi–Dirac function.

The third application dealt with the interaction of polymers with carbon nanotubes. The system size of a few thousand atoms made a QM calculation prohibitively expen-

sive. Besides, the polymer–nanotube interaction of interest is essentially nonbond in nature. Therefore, classical molecular mechanics with an accurate interatomic potential is sufficient to treat such interactions. Because the nanotube is stiff compared to the polymer, the nanotube atoms are held fixed during the simulation. Therefore, it was important to use an interatomic potential that is highly accurate for polymers. To this end we used the COMPASS Forcefield [21], which has been well validated for a large number of polymers both in the gas and in condensed phases.

3. Application Examples

3.1 Effect of adsorbates on the field emission from the tip of a metallic nanotube

Synthesis of carbon nanotubes with length-to-width ratio as large as 10^5, as well as advanced fabrication methods for generating self-aligned or patterned nanotube films on glass [22] or silicon [23] substrates have pushed nanotube-based flat-panel displays to the brink of commercial reality [24]. One major challenge to overcome is to reduce the operating voltage. One way to achieve this is to introduce adsorbates that might effectively lower the ionization potential (IP) and facilitate the extraction of electrons. An important experimental work in this regard was done at Motorola [25], in which changes in field emission behavior in the presence of various gases were studied, i.e., O_2, H_2 and water vapor. While O_2 and H_2 did not affect the field emission behavior appreciably, adsorbed water was found to significantly enhance the emission current.

3.1.1 Simulation setup

In order to understand the difference between H_2 and water on the field-emission properties of carbon nanotubes, we carried out first principles electronic structure calculations using the DFT code DMol[3]. For the metallic nanotube we chose a (5, 5) armchair tube, with a hemispherical tip represented by the half of a C_{60} molecule (buckyball). A uniform external field E_{FE}, directed toward the tube from above, was chosen to represent the electric field close to the tube tip under field emission conditions. Since the actual field close to the tip is radial rather than uniform [26], the uniform field representation is appropriate only if the tube-stem in the simulation is confined to the same size as the tube diameter. For this reason, a short stem of three atomic layers (30 atoms) was used. A more realistic field around the tip could perhaps be simulated by means of a large number of point charges situated at some distance from the tip. Such an effort was not undertaken for two reasons: (1) in all flat panel display designs the field emission occurs not from isolated tubes, but from a film of closely-spaced nearly-aligned tubes, with the resulting E-field more closely resembling a uniform field above the tip assembly; (2) the essential chemistry that drives the effect of adsorbates on field emission behavior can be extracted from calculations using a uniform field, as illustrated below. For all calculations a magnitude of $E_{FE} = 1$ V/Å was used as a ballpark figure around which field emission is known to occur for these systems. Difference in electronegativities between H and C introduces an artificial dipole moment in the nanotube if the dangling C atoms at the stem-end are H-saturated. The C atoms at the stem end were therefore left unsaturated. In addition, these C atoms were fixed during the simulation in order to mimic the presence of a long stem in actual experiments.

3.1.2 Results

The main results for this study can be summarized as follows:

a) A single H_2 molecule can either lie "flat" or "upright" on the nanotube. A single water molecule adsorbs in such a way that its plane symmetrically cuts the nanotube into two equal halves. The two H atoms are symmetrically equidistant from the tip, and could be either closer or further from the surface as compared to the O atom. We call these configurations "down" and "up" water, respectively.

b) At $E = 0$ none of the adsorbates show any significant binding to the nanotube tip. The H_2 has less than 0.1 kcal/mol binding in either configuration, while a single water has $\sim$0.7 kcal/mol binding.

c) At a tip-field of 1 V/Å, the binding energies change significantly. Thus, the H_2 has a binding energy of 1.1 and 3.5 eV in the flat and the upright configurations, respectively, while the "down" water has a binding energy of $\sim$20 kcal/mol, which is of the order of a chemical bond. The "up" water becomes unstable in the presence of a finite electric field at the nanotube and spontaneously flips into a "down" water. The "up" water is therefore not considered further in the discussion below.

d) Because water molecules can form clusters through H bonding, it was also important to consider the structure and adsorption energy of a cluster of water molecules on the nanotube tip. Because of the fivold symmetry of the (5, 5) nanotube (with a C_{60}-half cap) about its axis, it was easy for us to determine the global minimum for a cluster of five water molecules. In the minimum energy structure the five water molecules form a "crown" on the top of the nanotube (see Fig. 1). Each water molecule in this crown is tilted with respect to the ideal "down" water configuration for a single water (see point a) above). However, the resulting loss in interaction energy with the nanotube tip is almost exactly recovered from the gain in H bonding to the nearest neighbor waters [27].

e) The adsorbate atoms in all cases are at a distance of 3 Å or more from the nanotube surface. This strongly suggests that they are being physisorbed. This is supported by an analysis of charge density in the region between the adsorbate and the nanotube tip, which is less than 0.004 electrons/Å^3. Even at a field as large 1 V/Å, the changes to the adsorbate and nanotube structures are small. In particular, the distance between the adsorbate and the nanotube changes by less than 0.07 Å, and the bond-lengths change by less than 0.01 Å. The most significant geometrical change is in the H–O–H angle in

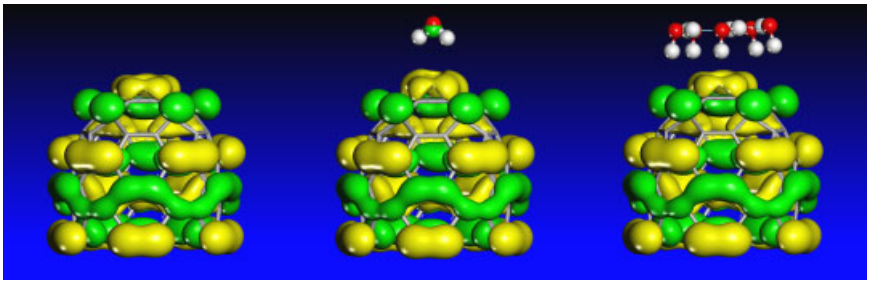


Fig. 1 (online colour). Highest Occupied Molecular Orbital (HOMO) for: isolated nanotube; nanotube +1 adsorbed water; and nanotube +5 adsorbed water. Although the position and shape of the HOMO is not affected significantly by the adsorbates, the energy level and ionization potential change markedly. See [27] for details

water, which decreases from 103.7° in $E = 0$ to 98° on the tube tip at $E_{FE} = 1$ eV/Å. Such a change in angle leads to only a 0.02 a.u. increase in the dipole moment of water.

f) An analysis of the various interaction energies and the dipole moments of the nanotube as well as the adsorbates yields the following picture: in the absence of an electric field, the nanotube has a very small dipole moment. This small dipole has only negligible interaction with any of the adsorbates. However, under field-emission conditions, the large E-field at the nanotube tip induces a significant dipole moment. This dipole interacts with the dipole of the adsorbates. Water molecules having a large intrinsic dipole moment interact strongly, while H_2 molecules have only a small field-induced dipole, and therefore a much weaker interaction.

g) Finally, we have analyzed the HOMO for the isolated nanotube, one water molecule on the nanotube, and five water molecules on the nanotube (Fig. 1). We find that the HOMO essentially remains confined to the nanotube tip, and its shape does not change significantly due to the presence of the adsorbates. However, when the ionization potential (IP) is computed, it is found to be 0.1 eV and 0.6 eV lower for the one water and five water case as compared to the adsorbate-free nanotube. This also correlates perfectly to the instability of the HOMO orbital [27]. Thus, electrostatic interactions from the adsorbates make the HOMO level in the nanotube more unstable, with a corresponding decrease in the Ionization Potential, thereby lowering the operating voltage for field emission.

3.2 Effect of mechanical deformation and chirality on phase-coherent transport through nanotubes

This study stems from the interest of using carbon nanotubes as nano-electromechanical sensors (NEMS). A pioneering experiment in this field is due to Tombler et al. [28], in which the middle part of the segment of a metallic nanotube suspended over a trench was pushed with an AFM tip. Beyond a deformation angle of $\sim 10°$ the electrical conductance of the tube dropped by more than two orders of magnitude. The effect was found to be completely reversible, i.e., through repeated cycles of AFM-deformation and tip removal, the electrical conductance displayed a cyclical variation with constant amplitude.

What interested us in this project was the theoretical explanation behind the conductance drop. The experimental drop in conductance was much higher than the computationally predicted values for tubes bent under mechanical duress. Such calculations, using both tight-binding [29] and semi-empirical Extended-Hückel type approaches [30] concluded that even under large bending angles the reduction in electrical conductance was less than an order of magnitude. For AFM-deformed nanotubes, in contrast, O(N) tight-binding calculations [31] show that beyond a critical deformation several C atoms close to the AFM tip become sp^3 coordinated. The sp^3 coordination ties up delocalized π electrons into localized σ states. This would naturally explain the large drop in electrical conductivity, as verified by explicit transport calculations.

3.2.1 Simulation setup

We investigated both types of deformation, i.e., deformation with an AFM tip and bending under mechanical duress. We also wanted to study the effect of tube chirality on the transport under deformation. To this end we considered a (12, 0) zigzag and a (6, 6) armchair tube, both of which are predicted to be metallic from electronic band-struc-

ture arguments. For the sake of comparison, we constructed both tubes out of 2400 atoms. For bending simulations, two halves of the tube were then rotated by equal and opposite angles about an axis perpendicular to the tube and passing through the center of mass of the initial straight tube. At each end of the tube, a contact region defined by a unit cell plus one atomic ring (a total of 36 and 60 atoms for the armchair and the zigzag tube, respectively) was then fixed and the whole tube relaxed with the UFF [14]. The AFM tip was modeled by a 6-layer deep 15-atom Li-needle normal to the (100) direction, terminating in an atomically sharp tip [32]. To simulate AFM-tip-deformation, the Li-needle was initially aimed at the center of a hexagon on the bottom-side of the middle part of tube. The Li-needle tip was then displaced by an amount δ toward the tube along the needle-axis, resulting in a deformation angle $\theta = \tan^{-1}(2\delta/L)$, L being the unstretched length of the tube. The whole tube was then relaxed by UFF, keeping the needle atoms and the end contact regions of the tube fixed. The contact region atoms were fixed in order to simulate an ideal undeformed semi-infinite carbon nanotube lead, and to ensure that all possible contact modes are coupled to the deformed part of the tube. Following the UFF relaxation, a cluster of 132 C atoms for the (6, 6) and a cluster of 144 C atoms for the (12, 0) were cut out from the middle of the tubes. These clusters, referred to below as the QM clusters (plus the 15 Li-tip atoms in tip-deformation simulations) were further relaxed with Accelrys' DFT-code DMol^3 [10], with the end atoms of the cluster plus the Li-tip atoms fixed at their respective classical positions. In order to cut down on CPU requirements, the DFT calculations were performed using the Harris functional [12], and the exchange-correlation potential due to Vosko et al. [33].

3.2.2 Results

The main results can be summarized as follows:

a) For bent tubes, even up to large bending angles (the maximum bending in our study was 40°), the tubes remained all-hexagonal. Beyond a critical angle (which depends on the size of the tube under study) a "kink" forms at the bottom side of the middle part of the tube to relieve the large strain. This result is in agreement with previous simulations using a different interatomic potential [34]. Explicit transport calculations confirmed that the conductance drop is small. Thus, at 40° bending, conductance for the (6, 6) armchair drops by only 1%. For the (12, 0) zigzag it is somewhat higher, being around 50%. None of these drops are significant enough for a sensitive electromechanical device.

b) Surprisingly, even under AFM-deformation, we found that the tubes remain all-hexagonal and each C atom remains essentially sp^2-coordinated. However, conductance drops are much higher than the bending case, particularly for the (12, 0) zigzag. Thus, at a deformation angle of 25°, the conductance for the (6, 6) tube drops by 5%, and that for the (12, 0) tube drops by a whopping four orders of magnitude, see Fig. 2.

c) The difference between the two types of deformations can be primarily attributed to a net elongation of the tube under AFM-deformation, and no net elongation under bending. Thus, the drop in conductance in the AFM-deformation experiment can be mimicked in a simpler (gedanken) experiment in which the tube is subjected to a uniform tensile strain [35].

d) The difference between the conductance behavior of armchair versus zigzag tubes can be attributed to the opening of a gap at the Fermi surface for a zigzag tube under

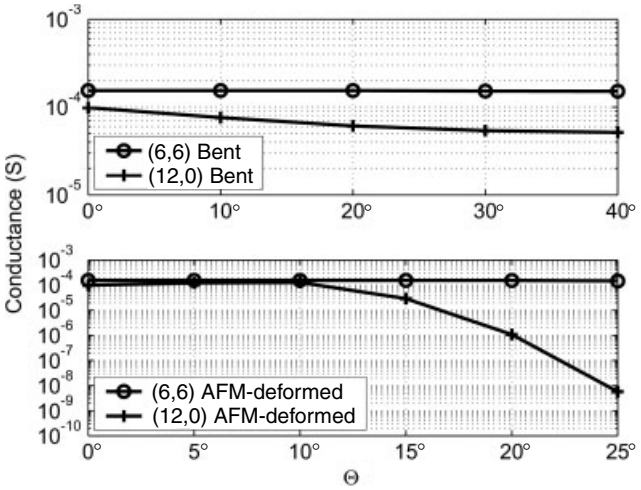


Fig. 2. Computed conductance (at $T = 300$ K) for the (6, 6) and (12, 0) nanotubes as a function of: (top) bending; and (bottom) tip-deformation. Under 40° bending conductance of the zigzag tube drops by a factor of 1.9, while for the armchair tube it drops by only 1.01. Under 25° tip-deformation, conductance of the zigzag tube drops by four orders of magnitude, while for the armchair tube it drops only by a factor of 1.05

stretch, while no such gap opens up for an armchair tube. Details are described elsewhere [35].

3.3 PmPV–nanotube interaction

Due to excellent mechanical properties of carbon nanotubes, nanotube-reinforced polymers are expected to have many properties superior to regular polymer composites. In fact, several groups have reported such experimental studies and increase, by as much as 20%, in both tensile and compressive moduli of an epoxy have been observed [36]. In order to optimize the properties of a polymer–nanotube composite, it is clearly important to understand the interaction between a nanotube and a polymer. Another motivation for such a study stems from the difficulty in processing nanotubes due to their insolubility in standard solvents. Based on their hydrophobic nature it was thought that nanotubes would dissolve in a hydrophobic solvent such as toluene. However, nanotubes readily form bundles and sediment out of toluene solution. It has been demonstrated that nanotubes can be rendered soluble using certain polymer matrices. One of the well-studied polymers in this regard is the poly(*m*–phenylenevinylene–co–2,5–dioctyloxy–*p*–phenylenevinylene) (PmPV) polymer, and a number of significant experiments in this regard have been carried out at the polymer research center, Trinity college, Dublin [37].

3.3.1 Experimental details

Single wall carbon nanotubes (SWNT) were produced using the arc discharge method. A solution of the polymer was prepared in toluene to a concentration of 1×10^{-5} M. To the solution, SWNT powder was added for different loading fractions (by mass).

The composite suspensions were sonicated for several minutes in a low power (60 W) sonic bath and then allowed to settle for a number of days. The resulting suspension was decanted from any settled solid. This suspension has been shown to be stable over indefinite periods (i.e. no subsequent settling of the material has been observed over a period of months). Raman studies [38] have shown an indication that the polymer–tube system increases the frequency of the modes by 21 cm^{-1} compared to 14 cm^{-1} for tube–tube interactions. Using these new amendments, the appropriate diameters have been calculated for each radial breathing mode (RBM) in the composite. It appears that the polymer interacts strongly with nanotubes within a diameter range of 1.3–1.5 nm and weakly with tubes of other diameters [38]. It should be noted that above 2% loading fraction, this selection process disappears. It is also dependent on the concentration of polymer in toluene. If the concentration is too high, the polymer aggregates and inhibits the interaction.

3.3.2 Simulation results and discussion

Previous simulations have shown that a long chain of PmPV polymer in the gas phase spirals itself into a helical arrangement [39]. This work found two low-energy configurations, with helix diameters 0.9 nm and 1.8 nm, respectively, the larger-diameter helix being slightly lower in energy. However, there are a few unsolved puzzles along the way. The inside of the gas phase helix is not "hollow", but rather stuffed with the octyloxy side groups. On the other hand, transmission electron microscopy indicates strong binding between PmPV and nanotubes [40]. However, the interaction of the polymer with the nanotube is not clear. TEM images have revealed both regular wrapping of the PmPV polymer around the nanotube, as well as structures without much order, with the later being more common.

As a first step in investigating this rather challenging problem, we considered the binding of a short segment, i.e., 4-mer of PmPV. For concreteness we chose helical nanotubes of chirality (12, 7) and (13, 6), both with diameter ∼1.3 nm. Chiral nanotubes were chosen in order to investigate the idea that the polymer might wrap the nanotube following the helical arrangement of hexagons on the nanotube surface. From preliminary molecular mechanics calculations using the COMPASS Forcefield [21] it appears that the diameter of the nanotube and not its helicity is the determining factor in the interaction with the polymer. The simulations also revealed that the polymer backbone provides the strongest binding (109 kJ per PmPV repeat) to the nanotubes, while the octyloxy side chains have significantly lower binding. Also, the backbone appears to be rigid in the sense that it costs energy to wrap it helically around the polymer. Rather it wants to run parallel to the nanotube axis, while the flexible side chains like to adjust themselves to the curvature of the nanotube surface (Fig. 3). However,

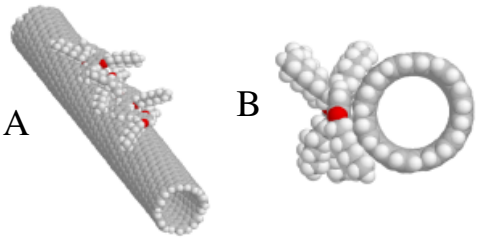


Fig. 3 (online colour). PmPV polymer (four repeat units) wrapped onto a (12, 7) carbon nanotubes in toluene solution. A: top view and B: side view. Carbon, hydrogen and oxygen atoms are shown in gray, white, and black, respectively

one needs to perform calculations using longer polymeric chains. In particular, it would be interesting to simulate structures and binding energies of nanotubes inserted into the helical structures of the pristine PmPV polymer. Such work is currently underway.

References

[1] S. Iijima, Nature **354**, 56 (1991).
S. Iijima, T. Ichihashi, and Y. Ando, Nature **356**, 776 (1992).
T. W. Ebbesen and P. M. Ajayan, Nature **358**, 220 (1992).
[2] D. S. Bethune et al., Nature **363**, 605 (1993).
S. Iijima and T. Ichihashi, Nature **363**, 603 (1993).
[3] Articles on nanotubes in: Phys. World **13**, Issue 6, 29 (2000).
[4] W. A. de Heer, A. Chatelain, and D. Ugarte, Science **270**, 1179 (1995).
A. G. Rinzler et al., Science **269**, 1550 (1995).
P. G. Collins and A. Zettl, Appl. Phys. Lett. **69**, 1969 (1996).
Y. V. Gulyaev et al., J. Vac. Sci. Technol. B **15**, 422 (1997).
S. Fan et al., Science **283**, 512 (1997).
O. M. Küttel, O. Groenig, C. Emmenegger, and L. Schlapbach, Appl. Phys. Lett. **73**, 2113 (1998).
M. J. Fransen, Th. L. van Rooy, and P. Kruit, Appl. Surf. Sci. **146**, 312 (1999).
S. Iijima, Nature **354**, 56 (1991).
[5] S. J. Tans, A. R. M. Verchueren, and C. Dekker, Nature **393**, 49 (1998).
[6] W. A. de Heer and R. Martel, Phys. World, June 2000, 49 (2000).
[7] C. Liu et al., Science **286**, 1127 (1999).
[8] Wong et al., Science **277**, 1971 (1997).
[9] H. Dai, Phys. World, June 2000, 43 (2000).
[10] http://www.accelrys.com/mstudio/dmol3.html
B. Delley, J. Chem. Phys. **92**, 508 (1990);
J. Phys. Chem. **100**, 6107 (1996).
[11] J. P. Perdew, K. Burke, and M. Ernzerhof, Phys. Rev. Lett. **77**, 3865 (1996).
[12] J. Harris, Phys. Rev. B **31**, 1770 (1985).
[13] Cerius^2 software, Accelrys Inc., San Diego, CA,
http://www.accelrys.com/doc/materials/cerius40/FFBSim/FF_SimulTOC.doc.html
[14] A. K. Rappe, C. J. Casewit, K. S. Colwell, W. A. Goddard, and W. M. Skiff, J. Am. Chem. Soc. **114**, 10024 (1992).
[15] N. Yao and V. Lordi, J. Appl. Phys. **84**, 1939 (1998).
[16] S. Datta, Electronic Transport in Mesoscopic Systems, Cambridge University Press, 1997.
[17] A. Svizhenko, M. P. Anantram, T. R. Govindan, B. Biegel, and R. Venugopal, J. Appl. Phys. **91**, 2343 (2002).
[18] D. A. Papaconstantopoulos, M. J. Mehl, S. C. Erwin, and M. R. Pederson, Tight-Binding Approach to Computational Materials Science, P. E. A. Turchi, A. Gonis, and L. Colombo (Eds.), MRS Proc. **491**, Materials Research Society, Warrendale, PA, 1998.
[19] In Eqs. (1) and (2), summation is performed over the repeating roman indices. The lower and upper indices denote covariant and contravariant components of a tensor.
[20] D. Lohez and M. Lanoo, Phys. Rev. B **27**, 5007 (1983).
[21] http://www.accelrys.com/mstudio/compass.html
H. Sun. and D. Rigby, Spectrochim. Acta A **53**, 1301 (1997).
[22] Z. F. Ren et al., Science **282**, 1105 (1998).
[23] S. Fan et al., Science **283**, 512 (1999).
[24] Q. H. Wang et al., Appl. Phys. Lett. **72**, 2912 (1998).
Y. Saito, S. Uemura, and K. Hamaguchi, Jpn. J. Appl. Phys., Part 2, **37**, L346 (1998).
Y. B. Choi et al., Appl. Phys. Lett. **75**, 3129 (1999).
[25] K. A. Dean, P. von Allmen, and B. R. Chalamala, J. Vac. Sci. Technol. B **17**, 1959 (1999).
[26] A. Maiti, C. J. Brabec, C. Roland, and J. Bernholc, Phys. Rev. Lett. **73**, 2468 (1994).
[27] A. Maiti, J. Andzelm, N. Tanpipat, and P. Von Allmen, Phys. Rev. Lett. **87**, 155502 (2001).

[28] T. W. TOMBLER et al., Nature **405**, 769 (2000).
[29] M. NARDELLI and J. BERNHOLC, Phys. Rev. B **60**, R16338 (1999).
[30] A. ROCHEFORT, P. AVOURIS, F. LESAGE, and D. SALAHUB, Phys. Rev. B **60**, 13824 (1999).
[31] L. LIU, C. S. JAYANTHI, and H. DAI, Phys. Rev. Lett. **84**, 4950 (2000).
[32] A. MAITI, phys. stat. sol. (b) **226**, 87 (2001).
[33] S. H. VOSKO, L. WILK, and M. NUSAIR, Can. J. Phys. **58**, 1200 (1980).
[34] S. IIJIMA, C. BRABEC, A. MAITI, and J. BERNHOLC, J. Chem. Phys. **104**, 2089 (1996).
[35] A. MAITI, A. SVIZHENKO, and M. P. ANANTRAM, Phys. Rev. Lett. **88**, 126805 (2002).
[36] L. S. SCHADLER, S. C. GIANNARIS, and P. M. AJAYAN, Appl. Phys. Lett. **73**, 3842 (1998).
[37] J. N. COLEMAN, S. CURRAU, A. B. DALTON, A. P. DAVEY, B. MCCARTHY, W. J. BLAU, and R. C. BARKLIE, Phys. Rev. B **58**, R7492 (1998).
[38] B. DALTON, C. STEPHAN, J. N. COLEMAN, B. MCCARTHY, P. M. AJAYAN, S. LEFRANT, P. BERNIER, W. J. BLAU, and H. J. BYRNE, J. Phys. Chem. B **104**, 10012 (2000).
[39] V. LORDI and N. YAO, J. Mater. Res. **15**, 2770 (2000).
[40] M. IN HET PANHUIS, A. MAITI, J. N. COLEMAN, A. B. DALTON, B. MCCARTHY, and W. J. BLAU, AIP Con. Proc. **591**, 497 (2001).